Electronic Supplement Information (ESI)

Energy landscape of polymorphic amyloid generation of β2-microglobulin revealed by calorimetry

Misaki Kinoshita[‡a], Yuxi Lin[‡b], Dai Itoh[a], Masaki Okumura[c], Natalia Markova[d], John E. Ladbury[e], Fabio Sterpone[f], Young-Ho Lee*[a]

[a]Institute for Protein Research, Osaka University, Yamadaoka 3-2, Suita, Osaka 565-0871, Japan.

[b]Department of Chemistry, Sookmyung Women's University, Cheongpa-ro 47-gil 100, Yongsan-gu, Seoul, 04310, Korea.

[c]Frontier Research Institute for Interdisciplinary Sciences (FRIS), Tohoku University, 6-3 Aramaki-Aza-Aoba, Aoba-ku, Sendai 980-8578, Japan.

[d]Malvern Panalytical, 22 Industrial Drive East, Northampton, MA, 01060, USA.

[e]School of Molecular and Cellular Biology, University of Leeds, Leeds, U.K.

[f]CNRS Laboratoire de Biochimie Théorique, Institut de Biologie Physico-Chimique, Université Paris Denis Diderot, Sorbonne Paris Cité, PSL Research University, 13 rue Pierre et Marie Curie, 75005, Paris, France.

[‡] These authors contributed equally to this work.

Corresponding author: Young-Ho Lee (E-mail: mr0505@protein.osaka-u.ac.jp)

Table of Contents

Supplementary Materials and Methods……..……...….3

Supplementary Discussion……..……...….6

Advantage of the ITC-based study on protein aggregation
Possible effects of shearing forces on the energy landscape
Perspectives of the energy landscape of protein aggregation

Supplementary Figures…...……...…….....10

Figure S1. **Reversibility of the thermal denaturation of β2m amyloid fibrils.**
Figure S2. **Thermodynamic and kinetic analyses of the ITC thermogram.**
Figure S3. **Dependencies of the lag time and rate constants for β2m amyloidogenesis on the stirring speed and the concentration of Ficoll.**
Figure S4. **ITC-based characterization of amyloid formation of D76N variant of β2m, amyloid β(1-40), and glucagon at 37 °C**
Figure S5. **Morphological analysis of β2m amyloid fibrils formed under the different stirring speeds.**
Figure S6. **Morphological analysis of β2m amyloid fibrils formed under the different concentrations of Ficoll.**
Figure S7. **One-dimensional proton NMR spectra of β2m monomer in the presence and absence of Ficoll.**

Supplementary References…..…….....19

Supplementary Materials and Methods

Reagents and proteins

Thioflavin T (ThT) and Ficoll 70 were obtained from Wako Pure Chemical Industries Ltd. (Osaka, Japan) and all other reagents were purchased from Nacalai Tesque (Kyoto, Japan). Recombinant human β_2-microglobulin (β2m) with an additional methionine residue at the N terminus was expressed in *Escherichia coli* and purified based on our previous study.[1] The concentration of β2m was determined using a molar extinction coefficient of 19,300 M^{-1} cm^{-1} at 280 nm.

Isothermal titration calorimetry measurements

Isothermal titration calorimetry (ITC) measurements for spontaneous amyloid formation of β2m of 3.5 mg ml^{-1} (297.6 μM) dissolved in 10 mM HCl solution (pH 2.0) were carried out using a PEAQ-ITC instrument (Malvern Panalytical, UK) at the desired stirring speeds and concentrations of Ficoll. 2.2 μl of the 10 mM HCl solution containing 1 M NaCl in the syringe was consecutively injected to the β2m monomer solution in the cell after a 15 min initial delay for thermal equilibration. In order to minimize the influence of residual bubbles and imperfect solution filling of the syringe, the first titration was conducted using 0.77 μl of solution in the syringe. Eleven NaCl titrations, spaced at intervals of 300 s, were performed with a duration of 1.54 s for the first titration and 4.4 s for the others to reach the final NaCl concentration of 100 mM. Changes in the heat flow were observed in real time with 10 μcal s^{-1} of reference power at 37 °C.

ThT assay

The formation of β2m amyloid fibrils was examined by a fluorometric assay of ThT at 37 °C. Excitation and emission wavelengths were 445 and 485 nm, respectively. 10 μl of aliquots were taken from the ITC cell following the incubation and mixed with 1.99 ml of 5 μM ThT in 50 mM glycine-NaOH buffer (pH 8.5). ThT fluorescence spectra were measured using a F7000 fluorescence spectrophotometer (Hitachi, Japan).

Circular dichroism measurements

Far-UV circular dichroism (CD) spectra of 0.1 mg ml^{-1} of β2m in 10 mM HCl solution (pH 2.0) containing 100 mM NaCl before and after ITC measurements at 37 °C were obtained using a JASCO J820 spectropolarimeter (Tokyo, Japan) and quartz cuvette with a 0.1-cm pathlength. Far-UV CD spectra of acid-denatured β2m monomers at 0.1 mg ml^{-1} in the absence and presence of Ficoll were also recorded in the same way. Reversibility of β2m amyloid fibrils between 37 and 100 °C was investigated at the heating rate of 1 °C min^{-1}. A cell holder equipped with a water circulator was used to keep the sample temperature constant at desired temperatures. Spectra were presented as mean residue ellipticity, [θ] (deg cm^2 $dmol^{-1}$), after subtraction of the solvent background.

Atomic force microscopy measurements

A 20-μl aliquot of the β2m sample solution diluted to 0.1 mg ml^{-1} following ITC measurements was applied to a mica plate. The residual solution was removed after 1 min, and the mica surface was washed twice using 200 μl of water and dried with compressed air. Atomic force microscopy (AFM) images were obtained using AFM5100N (Hitachi High-technologies, Tokyo, Japan). Distribution of the height of

amyloid fibrils formed at each condition was obtained by using Igor with an in-house algorithm.

Nuclear magnetic resonance measurements

One dimensional proton nuclear magnetic resonance (NMR) spectroscopy of β2m monomers at 1.18 mg ml^{-1} (100 μM) in 10 mM HCl solution (pH 2.0) containing 100 mM NaCl and 5% D_2O was recorded using the 400 MHz NMR spectrometer (Bruker BioSpin, Germany) equipped with a cryogenic probe at 37 °C and desired concentration of Ficoll. A standard pulse sequence with excitation sculpting (zgesgp from Bruker Topspin using the standard parameter set) was employed as this pulse sequence allows better suppression of the water signal with the excellent flat baseline through the selective excitation of H_2O during spin-echo and the use of purge gradients.[2] Data were processed using NMRPipe.[3]

Supplementary Discussion

Advantage of the ITC-based study on protein aggregation

Here we describe comprehensively merits of ITC for the study of protein aggregation compared to other techniques as follows.

1. ITC provides direct thermodynamic information on protein aggregation as evidenced by the previous[4-6] and current studies. Most of studies described thermodynamics using indirect experimental methods such as ThT assay and FT-IR. Computation/theory-based thermodynamics is practically difficult to be compared with direct experimental thermodynamics.
2. ITC can provide kinetic information on protein aggregation as suggested in the current study. Thus, one can obtain both kinetic and thermodynamic information in addition to some structural information (see below "8") at a time by performing a single ITC measurement.
3. Solubility and supersaturation of protein samples in the ITC cell are readily controlled by titrating samples in the ITC syringe, for instance, salts based on the Hofmeister series, as well as by changing the stirring speed.
4. Highly precise regulation of the temperature and stirring speed which can be useful as external stress/perturbation is possible.
5. By taking an advantage of function of titration, examination of spontaneous fibrillation and seeded fibrillation are both possible. In the case of seeded amyloid formation, by titrating of precursor monomers in the ITC syringe repeatedly to fibril seeds in the ITC cell, the precision (reproducibility) and accuracy of ITC results can be easily confirmed.

6. Effects of potent inhibitors on amyloid formation are readily evaluated by simply observing reaction of amyloid formation. The absence of reaction heat will indicate inhibition of amyloid formation while amyloid formation will show a clear exothermic ITC peak.
7. No immobilization and modification of samples are required.
8. Structural information of aggregates such as internal packing can be deduced based on ΔH in solution. Structural information of amyloid fibrils is still limited although solid-state NMR spectroscopy, X-ray/Cryo-ED, and Cryo-EM/Cyro-ET have suggested amyloid structures. However, all these techniques involve issues such as the lack of water molecules, crystal packing effects, and harsh treatment for sample preparation (e.g., low temperature), which may affect the structural and colloidal stability of amyloid fibrils and cause the change in morphology of amyloid fibrils.

Meanwhile, it is worthy while to mention the limitations of the ITC method. When reaction heat in the ITC thermogram is very small or exothermic and endothermic reactions occur almost simultaneously, detailed analysis and interpretation become difficult. Thus, formation of transient molecular species such as nuclei and oligomers with a very small amount of heat is hard to be traced using ITC. Markedly aggregation prone proteins which start to aggregate within the dead time of ITC measurements will not be proper for the ITC-based study.

Perspectives of the energy landscape of protein aggregation

The energy landscape provides comprehensive understanding of thermodynamic and kinetic properties of protein aggregation, and was used for conceptual explanation of the amyloid polymorphism.[7, 8] There have been simple energy landscapes. However, those

energy landscapes were constructed based on results obtained indirectly without using calorimetry-based direct thermodynamics. Temperature-dependent aggregation kinetics was used for obtaining information of the activation energy with a conventional ThT assay,[9-11] FT-IR,[12, 13] a quartz crystal oscillator,[14] or computation.[15-21] Temperature-dependent equilibrium constant (K_d or K_a) obtained using non-calorimetric approaches was also utilized for mapping an energy landscape.

In this study, we obviously showed a promise of the ITC-based energy landscape of amyloid generation in terms of thermodynamics and kinetics, and that our methodology is useful for revealing a property of amyloid aggregation, e.g., the polymorphism of amyloidogenesis. In order to build a more complete energy landscape, kinetic and thermodynamic characterization on the transition state and activation energy will be required with the ITC-based methodology. To this end, one needs to change temperature for ITC measurements and assume the absence of polymorphic amyloid formation. However, as suggested in the present study, changing ambient conditions for amyloid generation often induces polymorphism of amyloid fibrils.[22] Thus, the change in temperature may cause polymorphic amyloid generation, which in turn may not allow us to simply use the Arrhenius analysis based on the linearity (temperature-dependent kinetic constant). Despite of these marked difficulties, a perfect energy landscape which incorporates both thermodynamic and kinetic information will be highly challenging.

In addition, investigation of toxicity of different types of amyloid fibrils may be useful to correlate polymorphs of amyloid fibrils to the design of potential treatment of neurodegenerative diseases. In addition, examination of conformational and colloidal stability of each type of β2m amyloid fibril formed at different conditions will be also meaningful for leading to a potential cure of dialysis-related amyloidosis.

Possible effects of shearing forces on the energy landscape

Shearing force, which may mimic biological systems, is expected to affect protein aggregation and stability and is not considered to be artificial. Energy for stirring is fundamentally supplied from the ITC instrument. Shearing force itself and the change in the strength of the shearing force may affect amyloid aggregation. Difference in the strength of the shearing force may cause the formation of distinct types of nuclei, and thereby inducing the formation of different types of amyloid fibrils (i.e., polymorphic amyloid formation). There might be some energetic trades between shearing forces and nucleation although the examination of its mechanism is technically difficult. Indeed, agitation-induced formation of different types of insulin amyloid fibrils was reported.[23]

It should be noted that these energy trades, if any, could not be detected in ITC thermograms because nucleation must occur during the lag time. A future ITC instrument which can detect even smaller heat may improve our thermodynamic understanding of nucleation and its relationship with possible shearing-induced energy. Thus, shearing force can modify the energy landscape as it causes polymorphic amyloid generation, and does not impair the thermodynamic and kinetic analyses and interpretations in the current study.

Supplementary Figures

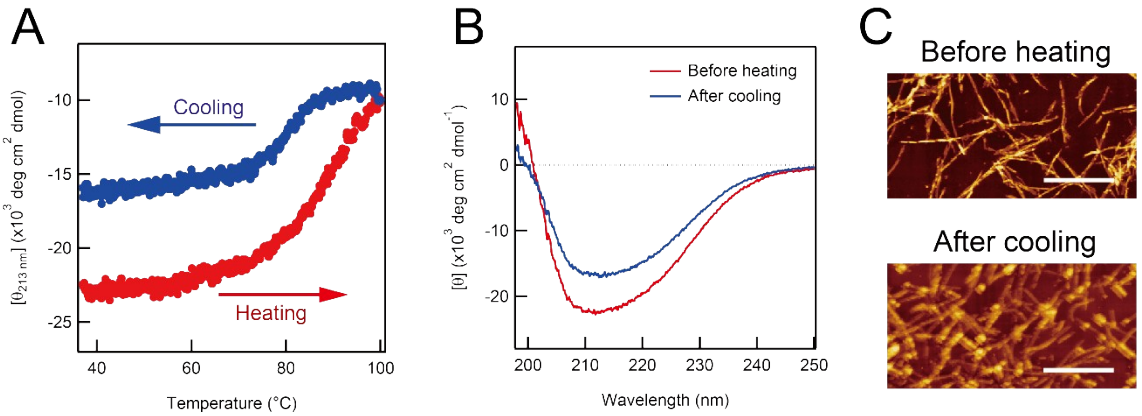

Figure S1. Reversibility of the thermal denaturation of β2m amyloid fibrils. (A) Heating (red) and cooling (blue) of the sample solution of β2m amyloid fibrils between 37 and 100 °C were traced with the CD intensity at 213 nm. (B and C) β2m amyloid fibrils before heating and after cooling were characterized using far-UV CD spectra (B) and AFM (C). The red and blue curves in *B* indicate the spectrum before and after the heating and subsequent cooling process, respectively. β2m amyloid fibrils melt to monomers at high temperature by showing the sigmoidal heat denaturation curve (red curve in *A*). Cooling down to 37 °C where amyloid fibrils were prepared restored the intensity of CD signal (A and B). A number of fibrillar aggregates following decreasing the temperature to 37 °C were detected in the AFM image. Thus, these results suggested that amyloid formation is a reversible process which ensured thermodynamic analyses. The difference in the CD signal may be ascribed to fibrillar association (thickening of fibrils) as observed in the AFM image.

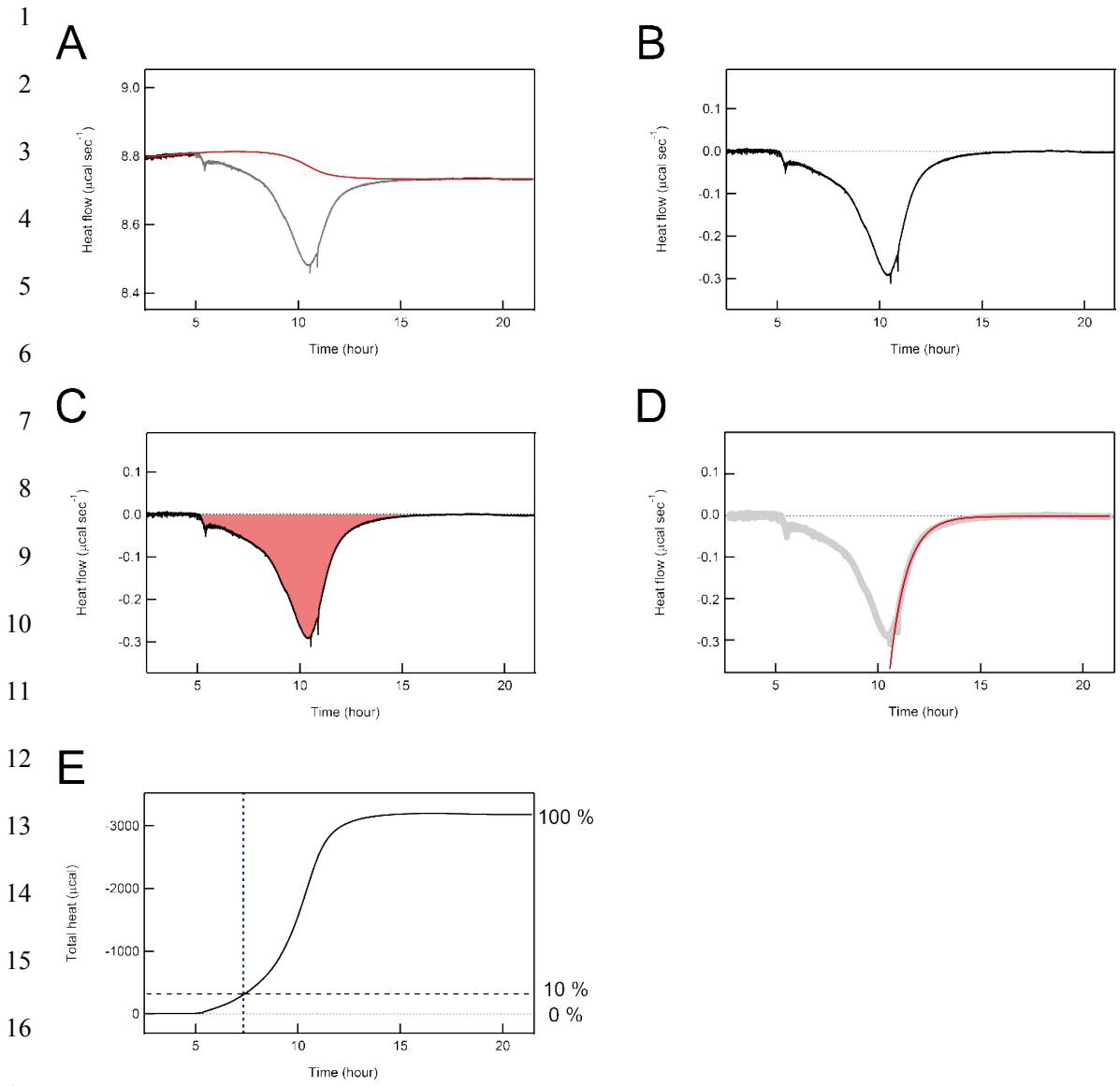

Figure S2. Thermodynamic and kinetic analyses of the ITC thermogram. (A and B) ITC thermograms before (A) and after (B) the baseline correction. The integral tangential baseline (red curve) was introduced for the baseline correction of the raw ITC thermogram (gray curve) in *A* as used in the baseline correction of the DSC thermogram. (C) The area of the ITC peak for integration is colored with red. (D) Elongation rate constant was obtained using the fit of the post-part of the ITC peak to the single exponential function (red curve). (E) Lag time was defined as the time point at which the

integrated heat reaches 10 % of the total heat. We previously defined the lag time of amyloid formation of β2m,[24] lysozyme,[25] insulin,[26] and amyloid β peptides[27] as the time point at which the intensity of ThT fluorescence reaches 10 % of the maximum ThT intensity.

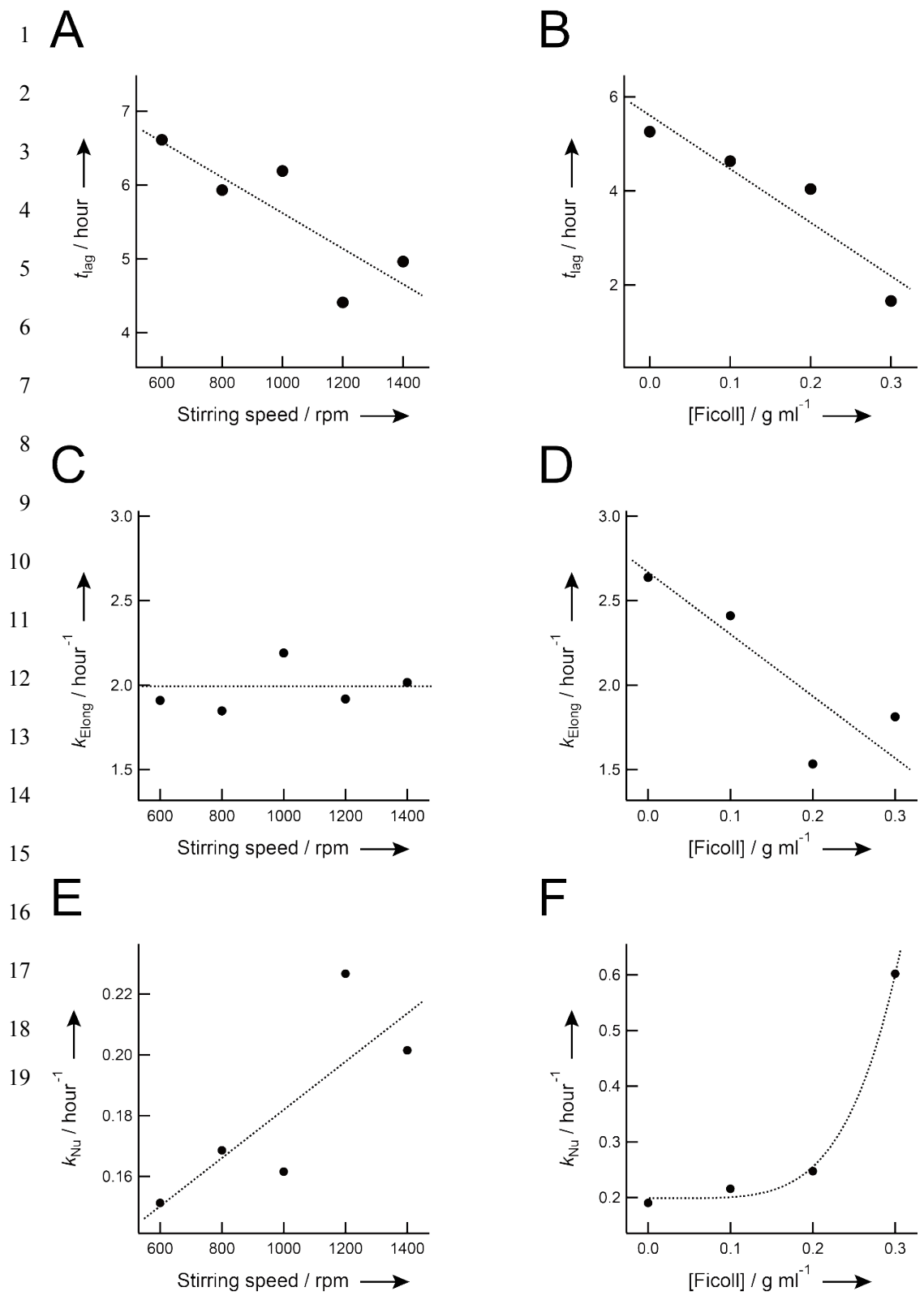
A
t_{lag} / hour
7
6
5
4
600
800
1000
1200
1400
Stirring speed / rpm
B
t_{lag} / hour
6
4
2
0.0
0.1
0.2
0.3
[Ficoll] / g ml^{-1}
C
k_{Elong} / hour^{-1}
3.0
2.5
2.0
1.5
600
800
1000
1200
1400
Stirring speed / rpm
D
k_{Elong} / hour^{-1}
3.0
2.5
2.0
1.5
0.0
0.1
0.2
0.3
[Ficoll] / g ml^{-1}
E
k_{Nu} / hour^{-1}
0.22
0.20
0.18
0.16
600
800
1000
1200
1400
Stirring speed / rpm
F
k_{Nu} / hour^{-1}
0.6
0.5
0.4
0.3
0.2
0.0
0.1
0.2
0.3
[Ficoll] / g ml^{-1}

Figure S3. Dependencies of the lag time and rate constants for β2m amyloidogenesis on the stirring speed and the concentration of Ficoll. (A-F) Lag times (t_{lag}) (A and B), elongation rate constants (k_{Elong}) (C and D), and nucleation rate constants (k_{Nu}) (E and F) were plotted as a function of the stirring speed at 37 °C (A, C, and E) and concentrations of Ficoll at 1,000 rpm and 37 °C (B, D, and F). Broken lines in *A*-*F* were drawn for eye-guide.

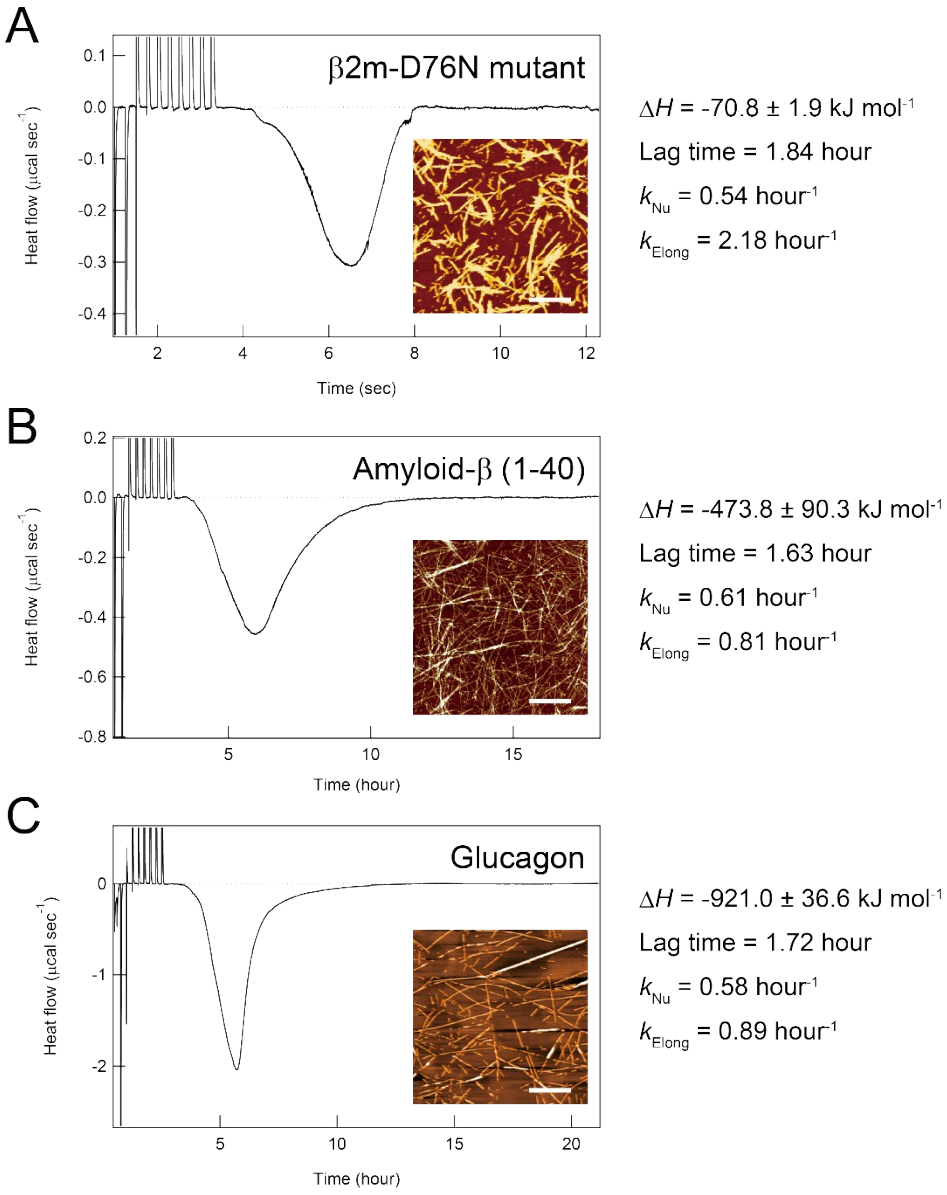

Figure S4. ITC-based characterization of amyloid formation of D76N variant of β2m, amyloid β(1-40), and glucagon at 37 °C. ITC thermograms of amyloid generation of D76N (1 mg ml^{-1}) (A) amyloid β(1-40) (0.15 mg ml^{-1}) (B), and glucagon (0.24 mg ml^{-1}) (C) at the stirring speed of 600 rpm are shown after the baseline correction. The final concentration of NaCl was 100 mM. ΔH, lag time, k_{Nu}, and k_{Elong} for amyloidogenesis of D76N (A) amyloid β(1-40) (B), and glucagon (C) are indicated. Each AFM image of sample solution after the incubation in the ITC cell is exhibited.

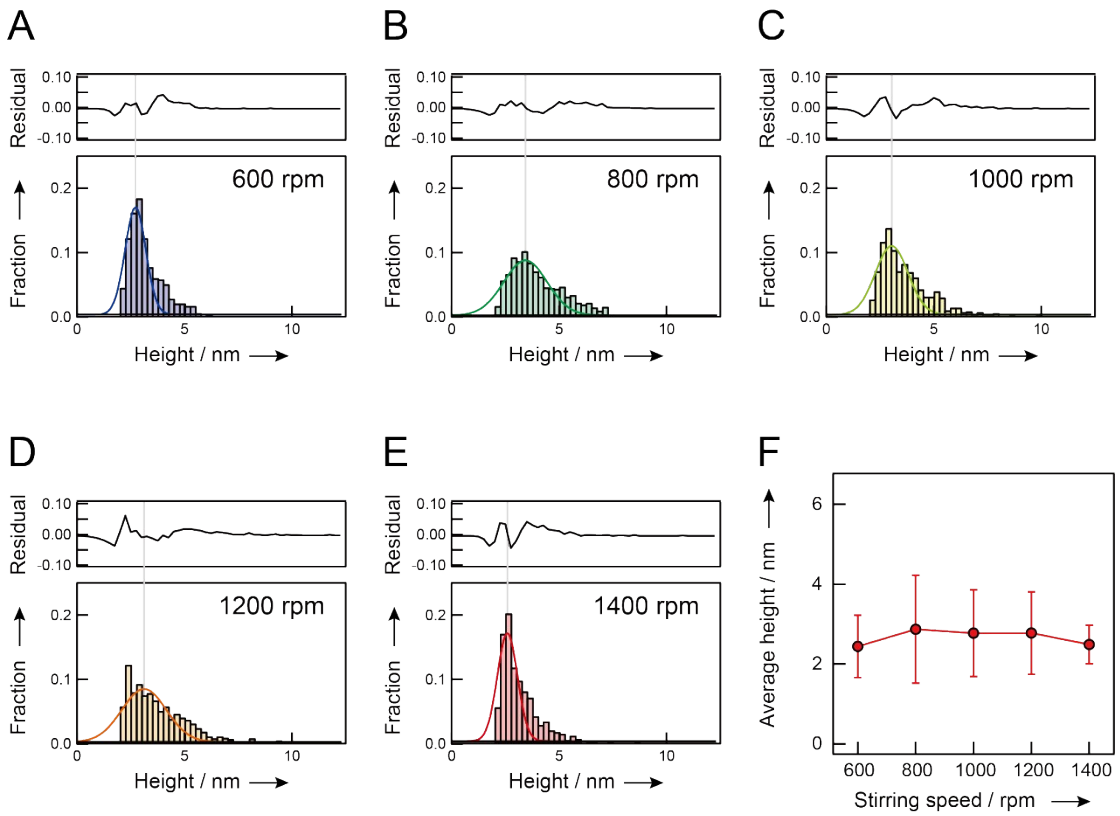

Figure S5. Morphological analysis of β2m amyloid fibrils formed under the different stirring speeds. (A-E) Distribution of the height of amyloid fibrils formed at 37 °C with the stirring speed of 600 (A), 800 (B), 1,000 (C), 1,200 (D), and 1,400 rpm (E) is shown. Fractions of fibrils with distinct heights are represented using histograms at lower panels. Best-fits to the Gaussian function are exhibited using color curves. Residuals of fit are shown at upper panels. The center of the Gaussian fit is indicated the vertical line. (F) Average values of the height of amyloid fibrils with standard deviations were plotted as a function of the stirring speed for generating amyloids.

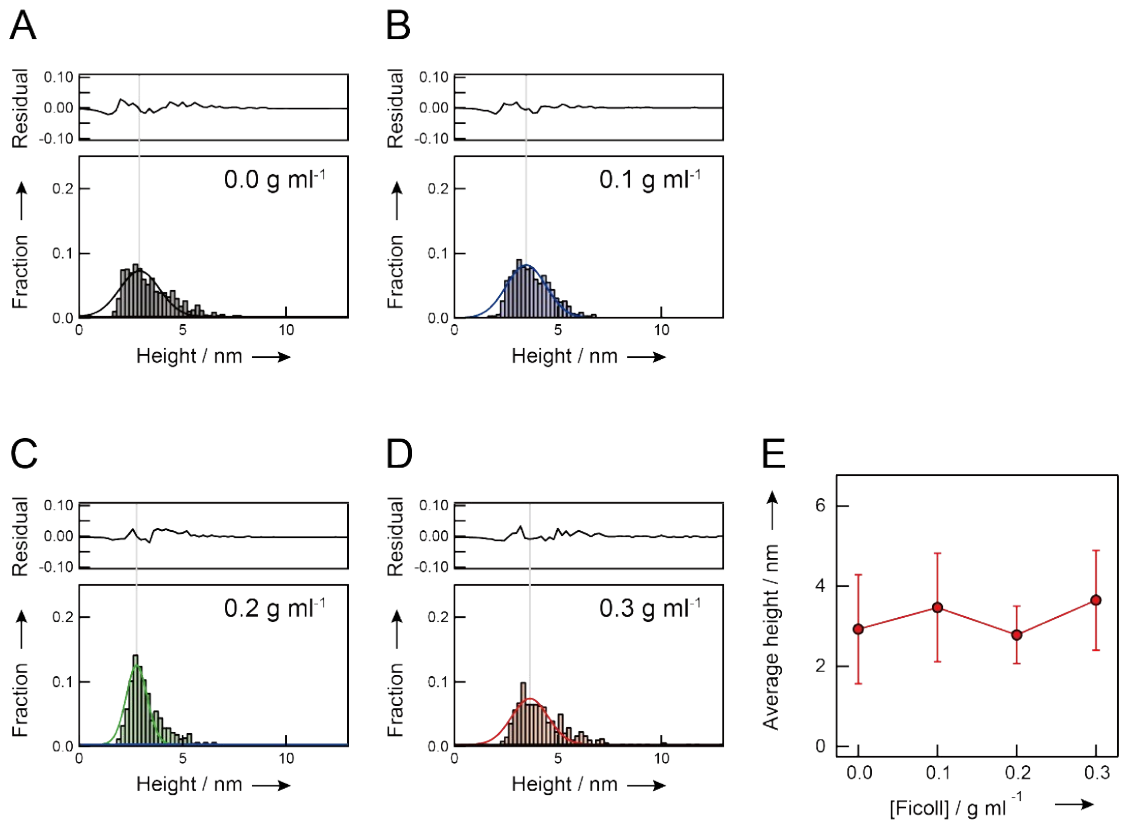

Figure S6. Morphological analysis of β2m amyloid fibrils formed under the different concentrations of Ficoll. (A-D) Distribution of the height of amyloid fibrils formed at 37 °C with the stirring speed of 1,000 rpm in the absence (A) and presence of Ficoll at 0.1 (B), 0.2 (C), and 0.3 g ml^{-1} (D). Fractions of fibrils with distinct heights are represented using histograms. Color curves indicate best-fits to the Gaussian function. Residuals of fit are shown at upper panels. The center of the Gaussian fit is indicated the vertical line. (E) Average values of the height of amyloid fibrils with standard deviations were plotted as a function of the concentration of Ficoll for ITC measurements.

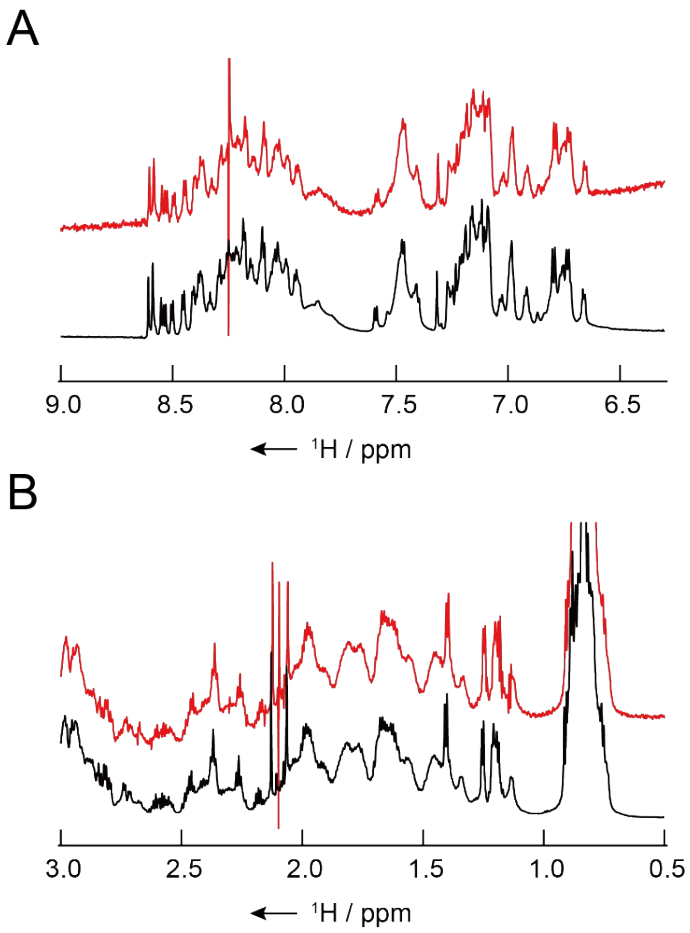

Figure S7. One-dimensional proton NMR spectra of β2m monomers in the presence and absence of Ficoll. (A and B) Solution NMR spectra of acid-unfolded β2m were collected at 37 °C in the absence (black) and presence of excess amounts of Ficoll (red). For better comparison, low and high field regions are separately represented for the main chain and aromatic residues (A) and for the methyl and methylene groups of side chains (B), respectively. NMR spectra after the subtraction of the spectrum of Ficoll are shown. Far-UV CD spectra without changing the uncharacteristic pattern and signal intensity (Fig. 2C) and no remarkable changes in the chemical shifts in one-dimensional proton NMR spectra for solution of β2m monomers were obtained, indicating no structural

changes of β2m monomers at the atomic and secondary structure level upon the addition of Ficoll.

Supplementary References

1 Y. H. Lee, E. Chatani, K. Sasahara, H. Naiki and Y. Goto, *J. Biol. Chem.*, 2009, **284**, 2169.

2 T. L. Hwang and A. J. Shaka, *J. Magn. Reson. A.*, 1995, **112**, 275.

3 F. Delaglio, S. Grzesiek, G. W. Vuister, G. Zhu, J. Pfeifer and A. Bax, *J. Biomol. NMR*, 1995, **6**, 277.

4 J. Kardos, K. Yamamoto, K. Hasegawa, H. Naiki and Y. Goto, *J. Biol. Chem.*, 2004, **279**, 55308.

5 M. D. Jeppesen, K. Hein, P. Nissen, P. Westh and D. E. Otzen, *Biophys. Chem.*, 2010, **149**, 40.

6 T. Ikenoue, Y. H. Lee, J. Kardos, H. Yagi, T. Ikegami, H. Naiki and Y. Goto, *Proc. Natl. Acad. Sci. U. S. A.*, 2014, **111**, 6654.

7 T. Eichner and S. E. Radford, *Mol Cell*, 2011, **43**, 8.

8 J. Adamcik and R. Mezzenga, *Angew. Chem. Int. Ed.*, 2018, DOI: 10.1002/anie.201713416.

9 R. Sabate, V. Castillo, A. Espargaro, S. J. Saupe and S. Ventura, *FEBS J.*, 2009, **276**, 5053.

10 M. Adachi, M. So, K. Sakurai, J. Kardos and Y. Goto, *J. Biol. Chem.*, 2015, **290**, 18134.

11 S. I. A. Cohen, R. Cukalevski, T. C. T. Michaels, A. Saric, M. Tornquist, M. Vendruscolo, C. M. Dobson, A. K. Buell, T. P. J. Knowles and S. Linse, *Nat. Chem.*, 2018, **10**, 523.

12 Viktor Farkas, Barbara Csordás, Orsolya Hegyi, Gábor K. Tóth and A. Perczel, *Eur. J. Org. Chem.*, 2013, **2013**, 3513.

13 A. L. Serrano, J. P. Lomont, L. H. Tu, D. P. Raleigh and M. T. Zanni, *J. Am. Chem. Soc.*, 2017, **139**, 16748.

14 T. P. Knowles, W. Shu, G. L. Devlin, S. Meehan, S. Auer, C. M. Dobson and M. E. Welland, *Proc. Natl. Acad. Sci. U. S. A.*, 2007, **104**, 10016.

15 C. Liu, M. Zhao, L. Jiang, P. N. Cheng, J. Park, M. R. Sawaya, A. Pensalfini, D. Gou, A. J. Berk, C. G. Glabe, J. Nowick and D. Eisenberg, *Proc. Natl. Acad. Sci. U. S. A.*, 2012, **109**, 20913.

16 W. Zheng, M. Y. Tsai, M. Chen and P. G. Wolynes, *Proc. Natl. Acad. Sci. U. S. A.*, 2016, **113**, 11835.

17 M. Chen, M. Tsai, W. Zheng and P. G. Wolynes, *J. Am. Chem. Soc.*, 2016, **138**, 15197.

18 W. Zheng, M. Y. Tsai and P. G. Wolynes, *J. Am. Chem. Soc.*, 2017, **139**, 16666.

19 Y. Sun, B. Wang, X. Ge and F. Ding, *Phys. Chem. Chem. Phys.*, 2017, **19**, 28414.

20 A. Rojas, N. Maisuradze, K. Kachlishvili, H. A. Scheraga and G. G. Maisuradze, *ACS Chem. Neurosci.*, 2017, **8**, 201.

21 K. Roder and D. J. Wales, *J. Am. Chem. Soc.*, 2018, **140**, 4018.

22 R. Tycko, *Protein Sci.*, 2014, **23**, 1528.

23 A. Loksztejn and W. Dzwolak, *J. Mol. Biol.*, 2010, **395**, 643.

24 Y. Yoshimura, Y. Lin, H. Yagi, Y. H. Lee, H. Kitayama, K. Sakurai, M. So, H. Ogi, H. Naiki and Y. Goto, *Proc. Natl. Acad. Sci. U. S. A.*, 2012, **109**, 14446.

25 Y. Lin, Y. H. Lee, Y. Yoshimura, H. Yagi and Y. Goto, *Langmuir*, 2014, **30**, 1845.

26 H. Muta, Y. H. Lee, J. Kardos, Y. Lin, H. Yagi and Y. Goto, *J. Biol. Chem.*, 2014, **289**, 18228.

27 M. Kinoshita, E. Kakimoto, M. S. Terakawa, Y. Lin, T. Ikenoue, M. So, T. Sugiki, A. Ramamoorthy, Y. Goto and Y. H. Lee, *Phys. Chem. Chem. Phys.*, 2017, **19**, 16257.